FRONTIERS OF PHYSICS

RESEARCH ARTICLE
Volume 18 / Issue 1 / 13307 / 2023

Moiré flat bands of twisted few-layer graphite

Zhen Ma[1], Shuai Li[1], Meng-Meng Xiao[1], Ya-Wen Zheng[1], Ming Lu[3,2], Haiwen Liu[5], Jin-Hua Gao[1,†], X. C. Xie[2,4]

1 School of Physics and Wuhan National High Magnetic Field Center, Huazhong University of Science and Technology, Wuhan 430074, China
2 International Center for Quantum Materials, School of Physics, Peking University, Beijing 100871, China
3 Beijing Academy of Quantum Information Sciences, Beijing 100193, China
4 CAS Center for Excellence in Topological Quantum Computation, University of Chinese Academy of Sciences, Beijing 100190, China
5 Center for Advanced Quantum Studies, Department of Physics, Beijing Normal University, Beijing 100875, China
Corresponding author. E-mail: †jinhua@hust.edu.cn
Received August 16, 2022; accepted October 19, 2022

ABSTRACT

We report that the twisted few layer graphite (tFL-graphite) is a new family of moiré heterostructures (MHSs), which has richer and highly tunable moiré flat band structures entirely distinct from all the known MHSs. A tFL-graphite is composed of two few-layer graphite (Bernal stacked multilayer graphene), which are stacked on each other with a small twisted angle. The moiré band structure of the tFL-graphite strongly depends on the layer number of its composed two van der Waals layers. Near the magic angle, a tFL-graphite always has two nearly flat bands coexisting with a few pairs of narrowed dispersive (parabolic or linear) bands at the Fermi level, thus, enhances the DOS at E_F . This coexistence property may also enhance the possible superconductivity as been demonstrated in other multiband superconductivity systems. Therefore, we expect strong multiband correlation effects in tFL-graphite. Meanwhile, a proper perpendicular electric field can induce several isolated nearly flat bands with nonzero valley Chern number in some simple tFL-graphites, indicating that tFL-graphite is also a novel topological flat band system.

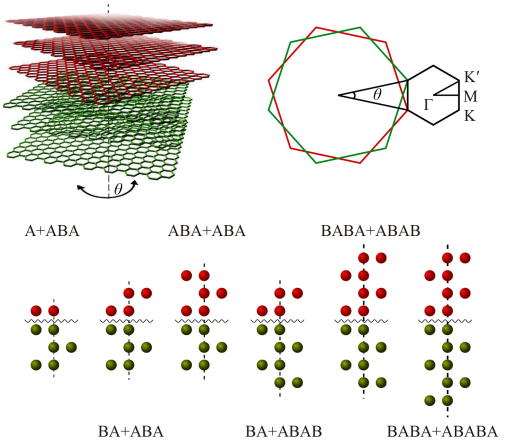

Keywords few-layer graphite, flat band, moiré heterostructures

1 Introduction

Moiré heterostructures (MHSs) have drawn great research interest recently [1–8]. The celebrated example is the twisted bilayer graphene (TBG), in which two atomically thin van der Waals (vdW) layers, i.e., graphene monolayers here, are stacked with a controlled twist angle θ. A small twist angle results in a long period moiré superlattice. Most importantly, the moiré interlayer hopping (MIH) will give rise to two nearly flat bands, when θ approaches the so-called magic angles [9–14]. Due to the divergent DOS of the moiré flat bands, exotic correlation phenomena, e.g., superconductivity and Mott insulator, have been observed in experiments [1–7], and intensively studied with various theoretical methods [15–28].

Further studies indicate that the moiré flat bands exist in a variety of MHSs, such as twisted double bilayer graphene [29–39], twisted trilayer graphene [40–47], twisted rhombohedral (ABC) multilayer graphene [48], trilayer graphene on boron nitride [49–51] and transition metal dichalcogenide heterostructures

Higher Education Press

arXiv: 2001.07995
https://doi.org/10.1007/s11467-022-1220-z

[52–57]. Note that, in all the above-mentioned MHSs, the low energy moiré band structures are in some sense similar, i.e., two moiré flat bands at Dirac Point isolated from other high energy bands. This is because that their vdW layers, like graphene monolayer, bilayer, ABC stacked multilayer, etc., just happen to have two low energy bands near the Fermi level E_F, which are hybridized by the MIH to form the two flat bands. In this work, we report a new family of moiré flat band systems, *twisted few-layer graphite* (tFL-graphite), which have richer and highly controllable moiré flat band structures entirely distinct from all the known MHSs. It is noteworthy that tFL-graphite has a similar band structure to double twisted trilayer garphene, which has been paid special attention to in recent experiments and was reported that unconventional superconductivity [58–60].

Typical tFL-graphites are shown in Fig. 1. Here, few layer graphite (FL-graphite) refers to multilayer graphene with Bernal (AB) stacking, in contrast to that with rhombohedral one. Generally, an $M + N$ tFL-graphite is composed of two FL-graphites (red and green in Fig. 1) stacked on top of each other with a twist angle θ, where M (N) is the layer number of the top (bottom) FL-graphite. We assume that $N \geq M$ without loss of generality, and only focus on the cases with $N \geq 3$. So, the simplest tFL-graphite here is the A + ABA (or 1 + 3) configuration, where A is the top monolayer (red) and ABA is the bottom ABA stacked trilayer (green) [see Fig. 1 (c)].

The distinct moiré band structure of tFL-graphite mainly results from the richer electronic structure of FL-graphite. It is known that an N-layer FL-graphite has $N/2$ electron-like bands and $N/2$ hole-like bands touching at the Dirac points if N is even, while an additional pair of linear bands appears for an odd N [62–64]. Thus, it is natural to expect a rather different moiré band structure in the tFL-graphite. And, as we will see later, twist actually has different influences on the bands of FL-graphite.

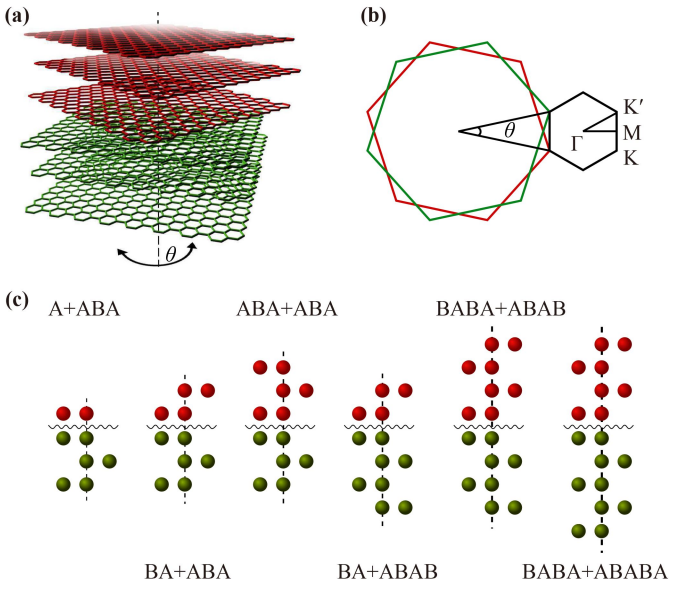

Fig. 1 **(a)** Schematic of the tFL-graphite, red (green) is the top (bottom) vdW layer. **(b)** Moiré Brillouin zone (black), red (green) is the first BZ of the top (bottom) vdW layer. **(c)** Side view of several tFL-graphite configurations.

We theoretically calculate the electronic structures of tFL-graphites based on a continuum model. Our results show that the electronic structure of a tFL-graphite strongly depends on the layer number of its composed vdW layers, which always has two moiré flat bands coexisting with a few pair of parabolic (or linear) narrow bands near the magic angle. For an $M + N$ tFL-graphite, the main characteristics of its moiré band structures are summarized as follows: (i) The number of the moiré bands at E_F is determined by N, i.e., the layer number of the thicker vdW layer, where it has N ($N + 1$) moiré bands if N is even (odd). (ii) Near the magic angle (about 1.05°), two of these moiré bands become flat, while others are still parabolic or linear at the Dirac points with narrowed bandwidth. (iii) We can get four isolated nearly flat bands with various nonzero valley Chern number by applying a proper electric field in the $N = 3$ cases.

Due to the unique electronic structures, the tFL-graphite has several great advantages as an intriguing MHS. (i) It has a richer and more flexible moiré band structure than the known MHSs, which can be dramatically changed by choosing different layer number. (ii) The coexistence of flat bands and other dispersive bands will not only enhance the density of states (DOS) at E_F, but also may meet the demand for the enhancement of superconductivity according to the steep band/flat band scenario [65, 66]. Both these two points imply that stronger multiband correlation effects, e.g., superconductivity at higher temperature, may occur in the tFL-graphite. (iii) It is a promising platform to study correlation effects in topological bands. (iv) The sample preparation of tFL-graphite may not be too challenging [67]. Note that natural graphite is Bernal stacked (more stable than the ABC graphene multilayers), and FL-graphite can be directly obtained by mechanical exfoliation.

2 Continuum model

Similar as the TBG, the required θ in the commensurate cases is determined by an integer m, where $\cos\theta = (3m^2 + 3m + \frac{1}{2})/(3m^2 + 3m + 1)$. The corresponding lattice vectors of the moiré supercell are $\boldsymbol{t}_1 = m\boldsymbol{a}_1 + (m+1)\boldsymbol{a}_2$ and $\boldsymbol{t}_2 = -(m+1)\boldsymbol{a}_1 + (2m+1)\boldsymbol{a}_2$, while $\boldsymbol{a}_1 = a(1/2, \sqrt{3}/2)$ and $\boldsymbol{a}_2 = a(-1/2, \sqrt{3}/2)$ are the lattice vectors of graphene with lattice constant $a \approx 0.246$ nm. The moiré Brillouin zone (BZ) is given in Fig. 1(b) (black), which

is determined by the BZ of the top vdW layer (red) and that of the bottom layer (green). The reciprocal lattice vectors G_i can be obtained from $\boldsymbol{G}_i \cdot \boldsymbol{t}_j = 2\pi\delta_{ij}$, and K (K') is the Dirac point corresponding to the top (bottom) layer [see Fig. 1 (b)].

The effective continuum model is used to describe the tFL-graphite [10–12]. For an $M + N$ tFL-graphite, the Hamiltonian is

$$H_{M+N}(\theta) = \begin{pmatrix} H_N(k_1) & T(r) \\ T^\dagger(r) & H_M(k_2) \end{pmatrix} + U, \tag{1}$$

where $k_1 = R(-\theta/2)(k - K)$, $k_2 = R(\theta/2)(k - K')$ and $R(\theta)$ is the rotation matrix. H_M (H_N) is the Hamiltonian of M-layer (N-layer) FL-graphite [62–64, 68]. For example, $H_{N=3}$ is the Hamiltonian of the ABA trilayer

$$H_{N=3}(k) = \begin{pmatrix} h_0(k) & g(k)^\dagger & 0 \\ g(k) & h_0(k) & g(k) \\ 0 & g(k)^\dagger & h_0(k) \end{pmatrix}, \tag{2}$$

where $h_0(\boldsymbol{k}) = -\hbar v_F \boldsymbol{k} \cdot \boldsymbol{\sigma}$ is the low-energy effective Hamiltonian for graphene monolayer and $g(k)$ is the interlayer hopping

$$g(k) = \begin{pmatrix} \hbar v_4 k_+ & \gamma_1 \\ \hbar v_3 k_- & \hbar v_4 k_+ \end{pmatrix}. \tag{3}$$

Here, $k_\pm = \xi k_x \pm \mathrm{i} k_y$, with $\xi = \pm 1$ for the two different valley in multilayer graphene. γ_1 is the vertical hopping and $v_i = \frac{\sqrt{3}\gamma_i a}{2\hbar}$ ($i = 3, 4$). γ_3 and γ_4 are the remote interlayer hoppings, which stand for the trigonal warping and electron-hole asymmetry, respectively. The moiré interlayer coupling is $T(r) = \sum_{n=0,1,2} T_n \cdot \mathrm{e}^{-\mathrm{i}Q_n \cdot r}$, where

$$T_n = I_{MN} \otimes \begin{pmatrix} \omega_1 & \omega_2 \mathrm{e}^{\mathrm{i}n\phi} \\ \omega_2 \mathrm{e}^{-\mathrm{i}n\phi} & \omega_1 \end{pmatrix}. \tag{4}$$

Here, I_{MN} is an $N \times M$ matrix with only one nonzero matrix element $I_{MN}(1, N) = 1$, $\phi = 2\pi/3$, $Q_n = R(n\phi) \cdot (K - K')$. At last, U in Eq. (1) is a diagonal matrix denoting the perpendicular electric field induced potential in layers, where we set the potential difference between adjacent two layers is V [61].

3 Moiré bands of the simplest tFL-graphite

Most of the moiré band characteristics of tFL-graphite can be seen from the simplest tFL-graphites, i.e., $N = 3$ and $M = (1, 2, 3)$. The calculated moiré bands are given in Fig. 2, each row of which corresponds to one structure of tFL-graphite. Here, we use a minimal model, only including the dominating interlayer hopping γ_1 in Eq. (3), to illustrate the ideal flat bands at the magic angle. We also use a full parameter model to account for the realistic situations, where the influence of γ_3 and γ_4 are considered [61]. The first to fourth columns in Fig. 2 are the moiré bands with $\theta = 3.88°$, $\theta = 1.33°$, $\theta = 1.05°$ and $\theta = 0.83°$, respectively. Corresponding DOS is also plotted.

First of all, tFL-graphite has more moiré bands than all the known MHSs at E_F. For example, all the cases ($N = 3$) in Fig. 2 have four moiré bands at E_F, instead of two like in TBG. It is because that the low energy

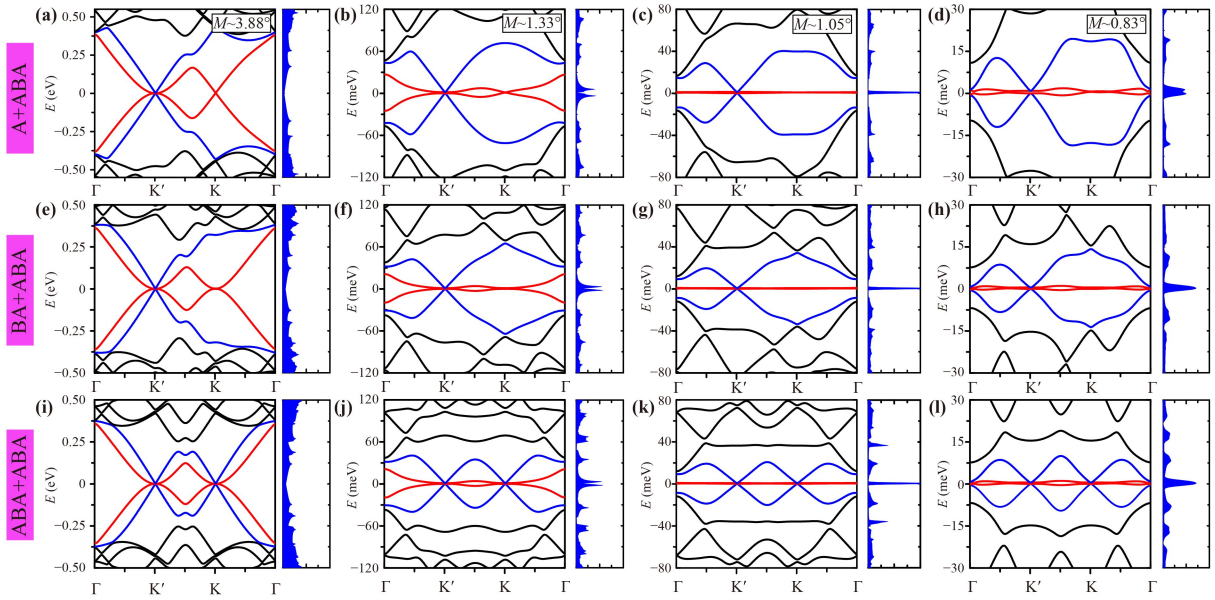

Fig. 2 **(a–d)**, **(e–h)** and **(i–l)** are the moiré bands of the A+ABA, BA+ABA and ABA+ABA, respectively. (a, e, i) are calculated at $\theta = 3.88°$; (b, f, j) are calculated at $\theta = 1.33°$; (c, g, k) are calculated at $\theta = 1.05°$; (d, h, l) are calculated at $\theta = 0.83°$. The moiré bands of AB+ABA and BAB+ABA are given in Ref. [61]. Red (blue) line indicate the first (second) conduction and valence bands respectively. Parameters: $\omega_1/\omega_2/\gamma_0/\gamma_1/\gamma_3/\gamma_4 = 78/98/2610/360/0/0$ meV, $\xi = -1$ [36, 48].

moiré bands of a tFL-grapite are constructed by hybridizing the bands of top and bottom vdW layers near the Dirac points via the MIH. In TBG, each vdW layer has two linear bands near the Dirac point. But in the A + ABA tFL-graphite, the top vdW layer (monolayer) has two linear bands, while the bottom vdW layer (ABA-trilayer) has four bands, i.e., a parabolic electron band, a parabolic hole band and a pair of linear bands. As shown in Figs. 2(a)–(d), the MIH hybridizes the two parabolic bands of the bottom ABA-trilayer with the two linear bands of the top monolayer (red lines), while the remaining two linear bands of the ABA-trilayer are modified into two other moiré bands at E_F (blue lines). Thus, there are four moiré bands near E_F in the A + ABA tFL-graphite. The moiré bands of BA + ABA [Figs. 2(e)–(h)] and ABA+ABA [Figs. 2(i)–(l)] tFL-graphites can be understood in a similar way. Generally, for an $M + N$ tFL-graphite, the number of moiré bands at E_F is equal to that of the thicker vdW layer, i.e., it has N moiré bands $(N+1)$ if N is even (odd) when $N \geq M$. Half of the moiré bands are electron-like and the others are hole-like.

The magic angle of the tFL-graphite is about 1.05°, the same as that of TBG. However, only two of these morié bands in tFL-graphite can be transformed into flat bands at the magnic angle, while others are still dispersive but their bandwidth are greatly narrowed. This is shown clearly in Figs. 2(c), (g) and (k), which are calculated with $\theta = 1.05°$ based on the minimal model. Increasing θ, the bandwidth of the moiré bands becomes larger, and the the flat bands become dispersive [see Figs. 2(b), (f), (j) with $\theta = 1.33°$]. With a twist angle smaller than the magic angle [e.g., $\theta = 0.83°$ in Figs. 2(d), (h) and (l)], the flat band [red lines] will become slightly dispersive while the bandwidth of the other two moiré bands [blue lines] are reduced further [smaller than 10 meV in Fig. 2(l)]. It suggests that the correlation in such narrow dispersive bands may be also very strong with small θ. At large twist angle [e.g., Figs. 2(a), (e) and (i) with $\theta = 3.88°$], the shape of the bands near K (K') points recovers to that of the isolated top (bottom) vdW layer. In order to figure out exactly where the flat bands distribute. we plot the wave functions of the flat band in A+ABA tFL-graphite at the Supplement [61]. The wave functions mainly distribute on both sides of the twisted interface (twisted layers), and there is almost no distribution far away from the twisted layers. Note that the A+ABA [Fig. 2(c)] and BA+ABA [Fig. 2(g)] both host flat bands coexisting with a single Dirac cone (K'), while ABA+ABA [Fig. 2(k)] have two Dirac cones. This coexistence feature is very interesting because that the simultaneous occurrence of flat and steep bands is a favorable condition to enhance superconductivity, according to the "steep band/flat band" scenario of superconductivity [65, 66]. Note that coexistence of flat band with linear bands at E_F was also noticed in some multi-twist MHSs very recently [43, 44, 69], while only one twist is required here. Due to existence of flat band and steep band, we believe tFL-graphite system will have the strongly correlated physics such as superconducting or correlated insulating states.

The low energy moiré bands of tFL-graphite also exhibit exotic topological properties, the valley Chern number of which can be nonzero. In Fig. 3, we consider two example, i.e., ABA + ABA and BAB + ABA. We first see that the four moiré bands at E_F can be isolated by a proper perpendicular electric field, while their bandwidth are still small. For these isolated moiré bands, we calculate their valley Chern numbers with the standard formula [61], which are indicated by black numbers in Fig. 3. The first interesting issue is that tFL-graphite here have four moiré bands with nonzero valley Chern number, while other known MHSs only have two [33, 34, 40, 48, 49]. Furthermore, despite that ABA + ABA and BAB+ABA differ only in the relative orientation and have very similar band structure [61], their moiré bands have different valley Chern number. The cases of AB + ABA and BA + ABA are similar, and the valley Chern number is controllable by the twist angle and perpendicular electric field [61].

4 Moiré bands of thicker tFL-graphite

Now we study the moiré bands of thicker tFG-graphites. Several typical examples are given in Fig. 4. These thicker tFL-graphites have various moiré bands near the E_F, depending on their own layer numbers. For example, with $N = 4$ (BA + ABAB, BABA + ABAB), there exists a pair of flat bands (red lines) coexisting with a parabolic electron and a parabolic hole bands (blue lines), as shown in Figs. 4(a, b) and (e, f). Compared with the $N = 3$ cases in Fig. 2, the parabolic bands here can obviously enhance the DOS at E_F. In general, higher DOS can always induce stronger correlation effects. It implies that correlation effects in thicker tFL-graphite may be stronger. However, more realistic facts

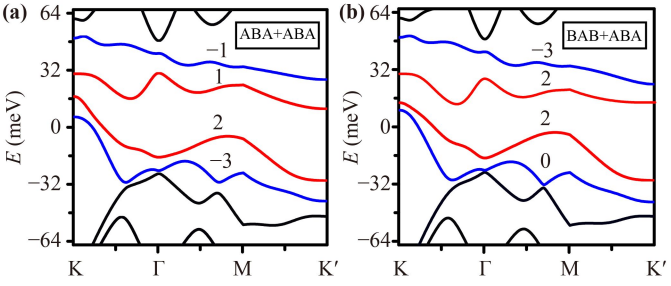

Fig. 3 **(a, b)** are the moiré bands under a perpendicular electric field for the ABA+ABA and BAB + ABA, respectively. $V = 20$ meV, $\theta = 1.33°$ and full parameter model is used. The black number are the valley Chern numbers for four moiré bands (red and blue solid lines).

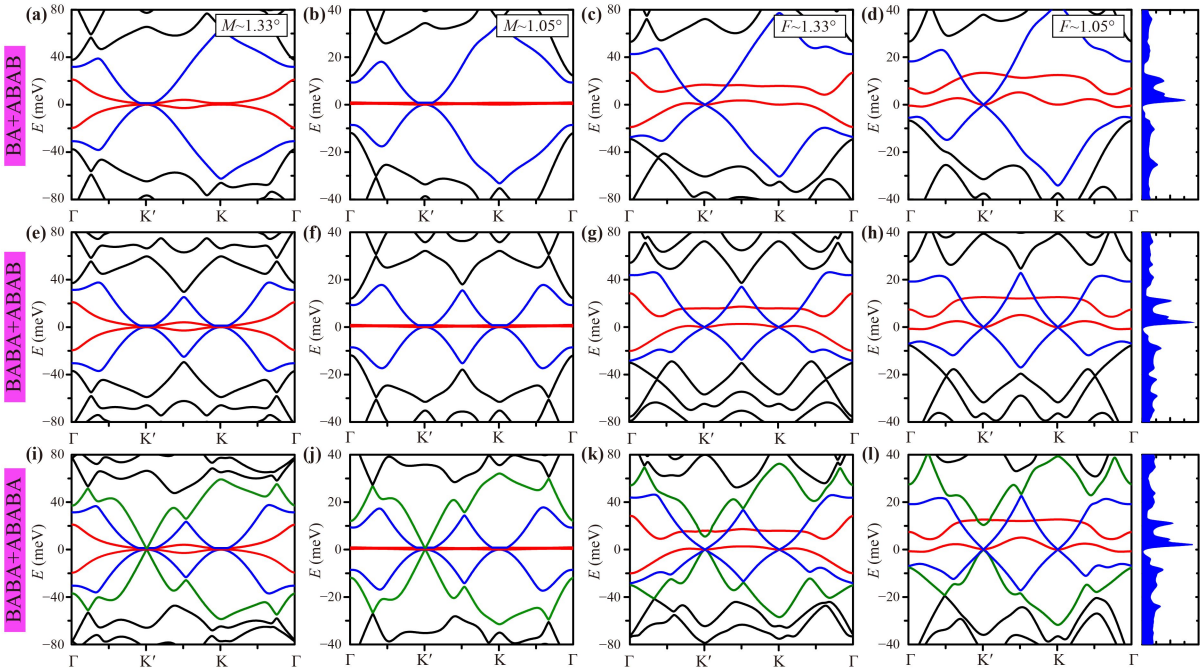

Fig. 4 **(a–d)**, **(e–h)** and **(i–l)** are the moiré bands of the BA+ABAB, BABA+ABAB and BABA+ABABA, respectively. (a, e, i) are calculated with the minimal model at $\theta = 1.33°$; (b, f, j) are calculated with minimal model at $\theta = 1.05°$; (c, g, k) are calculated with full parameter model at $\theta = 1.33°$; (d, h, l) are calculated with full parameter model at $\theta = 1.05°$, and the corresponding DOS is also plotted. Red (blue and green) line indicate the first(second and third) conduction and valence bands respectively. Parameters: $\omega_1/\omega_2/\gamma_0/\gamma_1/\gamma_3/\gamma_4 = 78/98/2610/360/283/138$ meV, $\xi = -1$.

should be considered for correlation effects in experiment. A detailed calculations (mean field for example) may be needed in future works. Increasing the layer number further, it is able to induce more moiré bands near the E_F. An $N = 5$ example is given in Figs. 4(i–j), which has six moiré bands including a pair of flat bands, two parabolic bands and two linear bands (green lines).

Note that the influence of the remote hopping γ_3 and γ_4 is critical, and different on various moiré bands, as illustrated by the full parameter model calculations in Figs. 4(c, d), (g, h) and (k, l). The remote hopping always separates the the flat bands in energy (red lines) and make them dispersive. But it does not significantly modify the parabolic bands near the Dirac points (blue lines). Meanwhile, a gap at the Dirac points is induced to the linear bands in $N = 5$ case [see in Figs. 4(k, l), green lines].

5 Summary

Our numerical calculations reveal and give some intuitive understanding about the unique, richer and highly controllable the moiré flat band structure in tFL-graphite, which may be directly verified by the nano-ARPES technique [70–73]. However, the research on the moiré bands in tFL-graphite is still at early stage, though the FL-graphite has been studied for rather a long time [67, 74–77]. Many basic problems are still unknown. For example, why does twist have different influences on the bands of FL-graphite? Whether can the multiband feature here significantly enhance the superconductivity? We hope our study will stimulate further interest on this promising system with moiré multiband correlations.

Note added The first draft of the article [arXiv: 2001.07995] was online in 2020. Subsequently, several works also study similar systems using various methods, and the results were consistent with ours [78–81].

Electronic supplementary material Supplementary materials are available in the online version of this article at https://doi.org/10.1007/s11467-022-1220-z and https://journal.hep.com.cn/fop/EN/10.1007/s11467-022-1220-z and are accessible for authorized users.

Acknowledgements We thank Jinhua Sun for helpful discussion. This work is supported by the National Natural Science Foundation of China (Grant Nos. 11874160, 12141401, and 11534001), the National Key Research and Development Program of China (Grant No. 2017YFA0403501), and the Fundamental Research Funds for the Central Universities (HUST: 2017KFYXJJ027).

References and notes

1. Y. Cao, V. Fatemi, A. Demir, S. Fang, S. L. Tomarken, J. Y. Luo, J. D. Sanchez-Yamagishi, K. Watanabe, T.

Taniguchi, E. Kaxiras, R. C. Ashoori, and P. Jarillo-Herrero, Correlated insulator behavior at half-filling in magic-angle graphene superlattices, *Nature* 556(7699), 80 (2018)
2. Y. Cao, V. Fatemi, S. Fang, K. Watanabe, T. Taniguchi, E. Kaxiras, and P. Jarillo-Herrero, Unconventional superconductivity in magic-angle graphene superlattices, *Nature* 556(7699), 43 (2018)
3. M. Yankowitz, S. Chen, H. Polshyn, Y. Zhang, K. Watanabe, T. Taniguchi, D. Graf, A. F. Young, and C. R. Dean, Tuning superconductivity in twisted bilayer graphene, *Science* 363(6431), 1059 (2019)
4. X. Lu, P. Stepanov, W. Yang, M. Xie, M. Aamir, I. Das, C. Urgell, K. Watanabe, T. Taniguchi, G. Zhang, A. Bachtold, A. MacDonald, and D. Efetov, Superconductors, orbital magnets and correlated states in magic-angle bilayer graphene, *Nature* 574(7780), 653 (2019)
5. A. Sharpe, E. Fox, A. Barnard, J. Finney, K. Watanabe, T. Taniguchi, M. Kastner, and D. Goldhaber-Gordon, Emergent ferromagnetism near three-quarters filling in twisted bilayer graphene, *Science* 365(6453), 605 (2019)
6. E. Codecido, Q. Wang, R. Koester, S. Che, H. Tian, R. Lv, S. Tran, K. Watanabe, T. Taniguchi, F. Zhang, M. Bockrath, and C. Lau, Correlated insulating and superconducting states in twisted bilayer graphene below the magic angle, *Sci. Adv.* 5(9), eaaw9770 (2019)
7. Y. Jiang, X. Lai, K. Watanabe, T. Taniguchi, K. Haule, J. Mao, and E. Andrei, Charge order and broken rotational symmetry in magic-angle twisted bilayer graphene, *Nature* 573(7772), 91 (2019)
8. Q. Tong, H. Yu, Q. Zhu, Y. Wang, X. Xu, and W. Yao, Topological mosaics in moiré superlattices of van der Waals heterobilayers, *Nat. Phys.* 13(4), 356 (2017)
9. J. M. B. Lopes dos Santos, N. M. R. Peres, and A. H. Castro Neto, Graphene bilayer with a twist: Electronic structure, *Phys. Rev. Lett.* 99(25), 256802 (2007)
10. R. Bistritzer and A. H. MacDonald, Moiré bands in twisted double-layer graphene, *Proc. Natl. Acad. Sci. USA* 108(30), 12233 (2011)
11. J. M. B. Lopes dos Santos, N. M. R. Peres, and A. H. Castro Neto, Continuum model of the twisted graphene bilayer, *Phys. Rev. B* 86(15), 155449 (2012)
12. P. Moon and M. Koshino, Optical absorption in twisted bilayer graphene, *Phys. Rev. B* 87(20), 205404 (2013)
13. M. Koshino, N. F. Q. Yuan, T. Koretsune, M. Ochi, K. Kuroki, and L. Fu, Maximally localized Wannier orbitals and the extended Hubbard model for twisted bilayer graphene, *Phys. Rev. X* 8(3), 031087 (2018)
14. J. Kang and O. Vafek, Symmetry, maximally localized Wannier states, and a low-energy model for twisted bilayer graphene narrow bands, *Phys. Rev. X* 8(3), 031088 (2018)
15. L. A. Gonzalez-Arraga, J. L. Lado, F. Guinea, and P. San-Jose, Electrically controllable magnetism in twisted bilayer graphene, *Phys. Rev. Lett.* 119(10), 107201 (2017)
16. C. Xu and L. Balents, Topological superconductivity in twisted multilayer graphene, *Phys. Rev. Lett.* 121(8), 087001 (2018)
17. H. C. Po, L. Zou, A. Vishwanath, and T. Senthil, Origin of Mott insulating behavior and superconductivity in twisted bilayer graphene, *Phys. Rev. X* 8(3), 031089 (2018)
18. H. Isobe, N. F. Q. Yuan, and L. Fu, Unconventional superconductivity and density waves in twisted bilayer graphene, *Phys. Rev. X* 8(4), 041041 (2018)
19. B. Padhi, C. Setty, and P. Phillips, Doped twisted bilayer graphene near magic angles: Proximity to Wigner crystallization, not Mott insulation, *Nano Lett.* 18(10), 6175 (2018)
20. F. Guinea and N. Walet, Electrostatic effects, band distortions, and superconductivity in twisted graphene bilayers, *Proc. Natl. Acad. Sci. USA* 115(52), 13174 (2018)
21. C. C. Liu, L. D. Zhang, W. Q. Chen, and F. Yang, Chiral spin density wave and $d+id$ superconductivity in the magic-angle-twisted bilayer graphene, *Phys. Rev. Lett.* 121(21), 217001 (2018)
22. H. Guo, X. Zhu, S. Feng, and R. T. Scalettar, Pairing symmetry of interacting fermions on a twisted bilayer graphene superlattice, *Phys. Rev. B* 97(23), 235453 (2018)
23. Y. P. Lin and R. M. Nandkishore, Kohn–Luttinger superconductivity on two orbital honeycomb lattice, *Phys. Rev. B* 98(21), 214521 (2018)
24. F. Wu, A. H. MacDonald, and I. Martin, Theory of phonon-mediated superconductivity in twisted bilayer graphene, *Phys. Rev. Lett.* 121(25), 257001 (2018)
25. B. Lian, Z. Wang, and B. A. Bernevig, Twisted bilayer graphene: A phonon-driven superconductor, *Phys. Rev. Lett.* 122(25), 257002 (2019)
26. T. J. Peltonen, R. Ojajärvi, and T. T. Heikkilä, Mean-field theory for superconductivity in twisted bilayer graphene, *Phys. Rev. B* 98(22), 220504 (2018)
27. D. M. Kennes, J. Lischner, and C. Karrasch, Strong correlations and $d+id$ superconductivity in twisted bilayer graphene, *Phys. Rev. B* 98(24), 241407 (2018)
28. Y. Z. You and A. Vishwanath, Superconductivity from valley fluctuations and approximate $SO(4)$ symmetry in a weak coupling theory of twisted bilayer graphene, *npj Quantum Mater.* 4(1), 16 (2019)
29. X. Liu, Z. Hao, E. Khalaf, J. Y. Lee, Y. Ronen, H. Yoo, D. Haei Najafabadi, K. Watanabe, T. Taniguchi, A. Vishwanath, and P. Kim, Tunable spin-polarized correlated states in twisted double bilayer graphene, *Nature* 583(7815), 221 (2020)
30. C. Shen, Y. Chu, Q. Wu, N. Li, S. Wang, Y. Zhao, J. Tang, J. Liu, J. Tian, K. Watanabe, T. Taniguchi, R. Yang, Z. Y. Meng, D. Shi, O. V. Yazyev, and G. Zhang, Correlated states in twisted double bilayer graphene, *Nat. Phys.* 16(5), 520 (2020)
31. Y. Cao, D. Rodan-Legrain, O. Rubies-Bigorda, J. M. Park, K. Watanabe, T. Taniguchi, and P. Jarillo-Herrero, Tunable correlated states and spin-polarized phases in twisted bilayer–bilayer graphene, *Nature* 583(7815), 215 (2020)
32. G. W. Burg, J. Zhu, T. Taniguchi, K. Watanabe, A. H. MacDonald, and E. Tutuc, Correlated insulating states in twisted double bilayer graphene, *Phys. Rev. Lett.* 123(19), 197702 (2019)
33. Y. H. Zhang, D. Mao, Y. Cao, P. Jarillo-Herrero, and T. Senthil, Nearly flat Chern bands in moiré superlattices,

Phys. Rev. B 99(7), 075127 (2019)
34. M. Koshino, Band structure and topological properties of twisted double bilayer graphene, *Phys. Rev. B* 99(23), 235406 (2019)
35. N. R. Chebrolu, B. L. Chittari, and J. Jung, Flat bands in twisted double bilayer graphene, *Phys. Rev. B* 99(23), 235417 (2019)
36. J. Y. Lee, E. Khalaf, S. Liu, X. Liu, Z. Hao, P. Kim, and A. Vishwanath, Theory of correlated insulating behaviour and spin-triplet superconductivity in twisted double bilayer grapheme, *Nat. Commun.* 10, 5333 (2019)
37. F. Haddadi, Q. Wu, A. J. Kruchkov, and O. V. Yazyev, Moiré flat bands in twisted double bilayer graphene, *Nano Lett.* 20(4), 2410 (2020)
38. F. Wu and S. Das Sarma, Ferromagnetism and superconductivity in twisted double bilayer graphene, *Phys. Rev. B* 101(15), 155149 (2020)
39. F. J. Culchac, R. B. Capaz, L. Chico, and E. Suarez Morell, Flat bands and gaps in twisted double bilayer grapheme, arXiv: 1911.01347 (2019)
40. Z. Ma, S. Li, Y. W. Zheng, M. M. Xiao, H. Jiang, J. H. Gao, and X. C. Xie, Topological flat bands in twisted trilayer grapheme, arXiv: 1905.00622 (2019)
41. W. J. Zuo, J. B. Qiao, D. L. Ma, L. J. Yin, G. Sun, J. Y. Zhang, L. Y. Guan, and L. He, Scanning tunneling microscopy and spectroscopy of twisted trilayer graphene, *Phys. Rev. B* 97(3), 035440 (2018)
42. E. Suárez Morell, M. Pacheco, L. Chico, and L. Brey, Electronic properties of twisted trilayer graphene, *Phys. Rev. B* 87(12), 125414 (2013)
43. X. Li, F. Wu, and A. H. MacDonald, Electronic structure of single-twist trilayer graphene, arXiv: 1907.12338 (2019)
44. S. Carr, C. Li, Z. Zhu, E. Kaxiras, S. Sachdev, and A. Kruchkov, Ultraheavy and ultrarelativistic Dirac quasiparticles in sandwiched graphenes, *Nano Lett.* 20(5), 3030 (2020)
45. S. Xu, M. M. Al Ezzi, N. Balakrishnan, A. Garcia-Ruiz, B. Tsim, C. Mullan, J. Barrier, N. Xin, B. A. Piot, T. Taniguchi, K. Watanabe, A. Carvalho, A. Mishchenko, A. K. Geim, V. I. Fal'ko, S. Adam, A. H. C. Neto, K. S. Novoselov, and Y. Shi, Tunable van Hove singularities and correlated states in twisted monolayer–bilayer graphene, *Nat. Phys.* 17(5), 619 (2021)
46. S. Chen, M. He, Y. H. Zhang, V. Hsieh, Z. Fei, K. Watanabe, T. Taniguchi, D. H. Cobden, X. Xu, C. R. Dean, and M. Yankowitz, Electrically tunable correlated and topological states in twisted monolayer–bilayer graphene, *Nat. Phys.* 17(3), 374 (2021)
47. H. Polshyn, J. Zhu, M. A. Kumar, Y. Zhang, F. Yang, C. L. Tschirhart, M. Serlin, K. Watanabe, T. Taniguchi, A. H. MacDonald, and A. F. Young, Electrical switching of magnetic order in an orbital Chern insulator, *Nature* 588(7836), 66 (2020)
48. J. Liu, Z. Ma, J. Gao, and X. Dai, Quantum valley Hall effect, orbital magnetism, and anomalous Hall effect in twisted multilayer graphene systems, *Phys. Rev. X* 9(3), 031021 (2019)
49. B. L. Chittari, G. Chen, Y. Zhang, F. Wang, and J. Jung, Gate-tunable topological flat bands in trilayer graphene boron-nitride moiré superlattices, *Phys. Rev. Lett.* 122(1), 016401 (2019)
50. G. Chen, L. Jiang, S. Wu, B. Lyu, H. Li, B. L. Chittari, K. Watanabe, T. Taniguchi, Z. Shi, J. Jung, Y. Zhang, and F. Wang, Evidence of a gate-tunable Mott insulator in a trilayer graphene moiré superlattice, *Nat. Phys.* 15(3), 237 (2019)
51. G. Chen, A. Sharpe, P. Gallagher, I. Rosen, E. Fox, L. Jiang, B. Lyu, H. Li, K. Watanabe, T. Taniguchi, J. Jung, Z. Shi, D. Goldhaber-Gordon, Y. Zhang, and F. Wang, Signatures of tunable superconductivity in a trilayer graphene moiré superlattice, *Nature* 572(7768), 215 (2019)
52. F. Wu, T. Lovorn, E. Tutuc, and A. H. MacDonald, Hubbard model physics in transition metal dichalcogenide moiré bands, *Phys. Rev. Lett.* 121(2), 026402 (2018)
53. M. H. Naik and M. Jain, Ultraflatbands and shear solitons in moiré patterns of twisted bilayer transition metal dichalcogenides, *Phys. Rev. Lett.* 121(26), 266401 (2018)
54. Y. Pan, S. Fölsch, Y. Nie, D. Waters, Y. C. Lin, B. Jariwala, K. Zhang, K. Cho, J. Robinson, and R. Feenstra, Quantum-confined electronic states arising from the moiré pattern of MoS_2–WSe_2 heterobilayers, *Nano Lett.* 18(3), 1849 (2018)
55. F. Wu, T. Lovorn, E. Tutuc, I. Martin, and A. H. MacDonald, Topological insulators in twisted transition metal dichalcogenide homobilayers, *Phys. Rev. Lett.* 122(8), 086402 (2019)
56. F. Conte, D. Ninno, and G. Cantele, Electronic properties and interlayer coupling of twisted MoS_2/$NbSe_2$ heterobilayers, *Phys. Rev. B* 99(15), 155429 (2019)
57. S. Javvaji, J. H. Sun, and J. Jung, Topological flat bands without magic angles in massive twisted bilayer graphenes, *Phys. Rev. B* 101(12), 125411 (2020)
58. J. M. Park, Y. Cao, K. Watanabe, T. Taniguchi, and P. Jarillo-Herrero, Tunable strongly coupled superconductivity in magic-angle twisted trilayer graphene, *Nature* 590(7845), 249 (2021)
59. Z. Hao, A. M. Zimmerman, P. Ledwith, E. Khalaf, D. H. Najafabadi, K. Watanabe, T. Taniguchi, A. Vishwanath, and P. Kim, Electric field–tunable superconductivity in alternating-twist magic-angle trilayer graphene, *Science* 371(6534), 1133 (2021)
60. M. Liang, M. M. Xiao, Z. Ma, and J. H. Gao, Moiré band structures of the double twisted few-layer graphene, *Phys. Rev. B* 105(19), 195422 (2022)
61. See the Supplemental Material for more details.
62. F. Guinea, A. H. Castro Neto, and N. M. R. Peres, Electronic states and Landau levels in graphene stacks, *Phys. Rev. B* 73(24), 245426 (2006)
63. M. Koshino and T. Ando, Orbital diamagnetism in multilayer graphenes: Systematic study with the effective mass approximation, *Phys. Rev. B* 76(8), 085425 (2007)
64. H. Min and A. H. MacDonald, Chiral decomposition in the electronic structure of graphene multilayers, *Phys. Rev. B* 77(15), 155416 (2008)
65. A. Simon, Superconductivity and chemistry, *Angew. Chem. Int. Ed. Engl.* 36(17), 1788 (1997)
66. A. Bussmann-Holder, H. Keller, A. Simon, and A. Bianconi, Multi-band superconductivity and the steep band/flat band scenario, *Condens. Matter* 4(4), 91 (2019)

67. J. B. Wu, X. Zhang, M. Ijäs, W. P. Han, X. F. Qiao, X. L. Li, D. S. Jiang, A. C. Ferrari, and P. H. Tan, Resonant Raman spectroscopy of twisted multilayer graphene, *Nat. Commun.* 5(1), 5309 (2014)
68. F. Zhang, B. Sahu, H. Min, and A. H. MacDonald, Band structure of ABC-stacked graphene trilayers, *Phys. Rev. B* 82(3), 035409 (2010)
69. E. Khalaf, A. J. Kruchkov, G. Tarnopolsky, and A. Vishwanath, Magic angle hierarchy in twisted graphene multilayers, *Phys. Rev. B* 100(8), 085109 (2019)
70. H. Peng, N. B. M. Schröter, J. Yin, H. Wang, T. F. Chung, H. Yang, S. Ekahana, Z. Liu, J. Jiang, L. Yang, T. Zhang, C. Chen, H. Ni, A. Barinov, Y. P. Chen, Z. Liu, H. Peng, and Y. Chen, Substrate doping effect and unusually large angle van Hove singularity evolution in twisted bi- and multilayer graphene, *Adv. Mater.* 29(27), 1606741 (2017)
71. M. I. B. Utama, R. J. Koch, K. Lee, N. Leconte, H. Li, S. Zhao, L. Jiang, J. Zhu, K. Watanabe, T. Taniguchi, et al., Visualization of the flat electronic band in twisted bilayer graphene near the magic angle twist, *Nat. Phys.* 17, 184 (2021)
72. J. J. P. Thompson, D. Pei, H. Peng, H. Wang, N. Channa, H. L. Peng, A. Barinov, N. B. M. Schröter, Y. Chen, and M. Mucha-Kruczy'nski, Determination of interatomic coupling between two-dimensional crystals using angle-resolved photoemission spectroscopy, *Nat. Commun.* 11(1), 3582 (2020)
73. S. Lisi, X. Lu, T. Benschop, T. A. de Jong, P. Stepanov, J. R. Duran, F. Margot, I. Cucchi, E. Cappelli, A. Hunter, A. Tamai, V. Kandyba, A. Giampietri, A. Barinov, J. Jobst, V. Stalman, M. Leeuwenhoek, K. Watanabe, T. Taniguchi, L. Rademaker, S. J. van der Molen, M. P. Allan, D. K. Efetov, and F. Baumberger, Observation of flat bands in twisted bilayer grapheme, *Nat. Phys.* 17, 189 (2021)
74. A. Vela, M. V. O. Moutinho, F. J. Culchac, P. Venezuela, and R. B. Capaz, Electronic structure and optical properties of twisted multilayer graphene, *Phys. Rev. B* 98(15), 155135 (2018)
75. T. Cea, N. Walet, and F. Guinea, Twists and the electronic structure of graphitic materials, *Nano Lett.* 19(12), 8683 (2019)
76. A. Grushina, D. K. Ki, M. Koshino, A. Nicolet, C. Faugeras, E. McCann, M. Potemski, and A. Morpurgo, Insulating state in tetralayers reveals an even–odd interaction effect in multilayer graphene, *Nat. Commun.* 6(1), 6419 (2015)
77. Y. Nam, D. K. Ki, D. Soler-Delgado, and A. Morpurgo, A family of finite-temperature electronic phase transitions in graphene multilayers, *Science* 362(6412), 324 (2018)
78. J. Wang and Z. Liu, Hierarchy of ideal flatbands in chiral twisted multilayer graphene models, *Phys. Rev. Lett.* 128(17), 176403 (2022)
79. Z. A. H. Goodwin, L. Klebl, V. Vitale, X. Liang, V. Gogtay, X. van Gorp, D. M. Kennes, A. A. Mostofi, and J. Lischner, Flat bands, electron interactions, and magnetic order in magic-angle mono-trilayer graphene, *Phys. Rev. Mater.* 5(8), 084008 (2021)
80. S. Zhang, B. Xie, Q. Wu, J. Liu, and O. V. Yazyev, Chiral decomposition of twisted graphene multilayers with arbitrary stacking, arXiv: 2012.11964 (2020)
81. X. Lin, H. Zhu, and J. Ni, Emergence of intrinsically isolated flat bands and their topology in fully relaxed twisted multilayer graphene, *Phys. Rev. B* 104(12), 125421 (2021)